
UNIVERSITY
OF WOLLONGONG
AUSTRALIA

University of Wollongong
Research Online

Faculty of Engineering - Papers (Archive) Faculty of Engineering and Information Sciences

2008

Electrochemistry of LiV3O8 nanoparticles made by flame spray pyrolysis

T J. Patey
Paul Scherrer Institute

See How Ng
Paul Scherrer Institute, shn076@uow.edu.au

R Buchel
Department of Mechanical and Process Engineering, Switzerland

N Tran
Paul Scherrer Institute

F Krumeich
Laboratory of Inorganic Chemistry, Switzerland

See next page for additional authors

http://ro.uow.edu.au/engpapers/2861

Publication Details

Patey, T. J., Ng, S., Buchel, R., Tran, N., Krumeich, F., Wang, J., Liu, H. K. Novak, P. (2008). Electrochemistry of LiV3O8 nanoparticles made by flame spray pyrolysis. Electrochemical and Solid-State Letters, 11 (4), A46-A50.

Research Online is the open access institutional repository for the University of Wollongong. For further information contact the UOW Library: research-pubs@uow.edu.au

Authors
T J. Patey, See How Ng, R Buchel, N Tran, F Krumeich, Jiazhao Wang, Hua-Kun Liu, and P Novak

This journal article is available at Research Online: http://ro.uow.edu.au/engpapers/2861

Electrochemical and Solid-State Letters, **11** (4) A46-A50 (2008)
1099-0062/2008/11(4)/A46/5/$23.00 © The Electrochemical Society

Electrochemistry of LiV_3O_8 Nanoparticles Made by Flame Spray Pyrolysis

T. J. Patey,[a,*] S. H. Ng,[a,b,*] R. Büchel,[c] N. Tran,[a] F. Krumeich,[d] J. Wang,[b] H. K. Liu,[b,] and P. Novák[a,**,z]**

[a]*Electrochemistry Laboratory, Paul Scherrer Institut, CH-5232 Villigen PSI, Switzerland*
[b]*Institute for Superconducting & Electronic Materials and ARC Centre of Excellence for Electromaterials Science, University of Wollongong, NSW 2522, Australia*
[c]*Particle Technology Laboratory, Department of Mechanical and Process Engineering, ETH Zurich, CH-8092 Zurich, Switzerland*
[d]*Laboratory of Inorganic Chemistry, ETH Zurich, CH-8093 Zurich, Switzerland*

LiV_3O_8 nanoparticles (primary particles with ca. 50 nm diameter) have been synthesized by flame spray pyrolysis (FSP). The powder was characterized by X-ray diffraction, scanning electron microscopy, transmission electron microscopy, and galvanostatic cycling. The initial discharge capacity of the LiV_3O_8 nanoparticles is 271 mAh g^{-1} when discharged from its open-circuit potential to 2.0 V vs Li/Li^+ at a specific current of 100 mA g^{-1} under ambient conditions. The nanoparticles retained a specific discharge capacity of 180 mAh g^{-1} beyond 50 cycles. This paper describes the synthesis route as well as the characterizations of the FSP-produced LiV_3O_8 nanoparticles.
© 2008 The Electrochemical Society. [DOI: 10.1149/1.2836741] All rights reserved.

Manuscript received September 27, 2007; revised manuscript received December 21, 2007.
Available electronically January 28, 2008.

Lithium-ion (Li-ion) rechargeable batteries are currently used in commercially available electronic devices due to their high cell voltage and energy density. $LiCoO_2$ is the current cathode material of choice; however, there is a demand for alternative cathode materials due to the high cost,[1,2] relative toxicity, and safety concerns of this material. LiV_3O_8 as a cathode material has the advantages of higher specific charge, lower cost, and better safety features.[3] An extensive amount of study has been conducted in topics including the material's degree of crystallinity,[4-6] the origin of capacity fading,[7] numerous synthesis methods,[3,8-10] and the polymer binder content in the composite electrode.[11,12]

The power density of Li-ion batteries can be improved by increasing the interfacial area between the electrolyte and the active material. The use of oxide nanoparticles as cathode materials in Li-ion batteries presents numerous opportunities and challenges.[13] There is an opportunity to increase the power density and at the same time the challenge in dealing with increased electrode–electrolyte side reactions. Both phenomena are due to the higher specific surface area of the nanoparticles compared to their μm-sized counterparts.

Flame spray pyrolysis (FSP) is a process which can produce oxide nanoparticles at an industrial scale. It is a flexible and scalable process[14,15] which is already used to produce fine powders for use as catalysts, coatings, and dental fillers, to name a few. FSP has been used previously to produce electrochemically active crystalline oxide nanoparticles with a spinel structure ($LiMn_2O_4$, $LiFe_5O_8$, and $Li_4Ti_5O_{12}$).[16] It is demonstrated that FSP is a potentially cost-effective process to producing electrochemically active nanosized spinel materials of controlled composition, crystallinity, and morphology. Furthermore, FSP has also been used to produce $LiCoO_2$.[17] All these advantages make FSP an attractive process to produce nanosized cathode materials.

This paper describes the synthesis of nanosized LiV_3O_8 material by FSP and presents the electrochemical characterization of this powder.

Experimental

The experimental setup for FSP is described elsewhere.[14] The precursor used for the flame synthesis was prepared by first dissolving 9.17 g of vanadium (V) oxytripropoxide (Aldrich, 98%) into 18.7 mL of diethylene glycol (Fluka). This solution was then stirred into 19.0 mL of toluene (Riedel-de Haën) and 12.5 mL of 1.0 M lithium tert-butoxide solution in tetrahydrofuran (Aldrich). Therefore, the precursor solution contains a molar ratio of Li to V of 1 to 3. Subsequently, this precursor was injected at a rate of 3 mL min^{-1} through the reactor nozzle and dispersed with 5 L min^{-1} of oxygen into a fine spray. A pressure of 1.5 bar was maintained across the nozzle tip. A premixed flame composed of 1 L min^{-1} of methane and 2 L min^{-1} of oxygen was maintained to ignite and support the combustion of the spray. A sheath gas of 5 L min^{-1} of oxygen surrounding the flame was used to ensure complete combustion. The dry powder was collected by placing a glass fiber filter (GF/D Whatman, 257 mm in diameter) above the flame and drawing the gas streams with a vacuum pump. The reactor was cooled by water to prevent overheating of the nozzle and precursor evaporation within the liquid feed lines. Additional precursors were prepared and tested with the same Li to V molar ratio, but with varying molar concentrations of the precursor solutions. This was done to provide an initial overview of the lab-scale powder production capability of FSP for the LiV_3O_8 nanoparticles.

The Brunauer–Emmett–Teller (BET) specific surface area (SSA) of the FSP-produced powder was determined through a five-point nitrogen adsorption isotherm at 77 K (Tristar, Micrometrics Instruments Corp.) after degassing the powder samples with nitrogen at 150°C. The X-ray diffraction (XRD) measurements were performed using a Bruker AXS D8 Advance (40 kV, 40 mA) and analyzed with the Topas 2 software. The XRD measurement was performed at a continuous scan between 2θ angles of 10 and 70° at a scan rate of 0.03° min^{-1}. Analysis by scanning electron microscopy (SEM) was performed with a Zeiss Gemini 1530 operated at 1 kV. For the investigation by transmission electron microscopy (TEM), the material was deposited onto a holey carbon foil supported on a copper grid. TEM investigations were performed using a CM30ST microscope (Philips; LaB_6 cathode, operated at 300 kV, point resolution ~2 Å). Elemental analysis was conducted using the inductively coupled plasma optical emission spectrometry (ICP-OES) method.

A mixture of the LiV_3O_8 powder and two types of carbon black (Super P and ENSACO 350, TIMCAL SA) [7:1:1 by weight] were dispersed within an organic solution of N-methylpyrrolidinone (NMP, Fluka). This suspension was then added to a solution composed of 10 wt % polyvinylidene fluoride (SOLEF PVDF 1015, Solvay) dissolved in NMP, forming a viscous slurry. The slurry was doctor bladed at a thickness of 200 μm onto an aluminum foil and dried under vacuum at 110°C overnight in order to remove the

* Electrochemical Society Student Member.
** Electrochemical Society Active Member.
z E-mail: petr.novak@psi.ch

solvent and form a composite electrode. The active material, LiV_3O_8, accounted for 70 wt % of the electrode composite.

Electrodes with a diameter of 13 mm were punched out and dried in a vacuum chamber at 120°C overnight. They were then assembled in test cells similar to coin cells,[18] where they functioned as the working electrode. Lithium metal (Aldrich, 99.9%) was used as both the counter and reference electrodes. It was separated from the working electrode by a 1 mm thick fiberglass separator soaked in 500 μL of electrolyte [ethylene carbonate (EC)/dimethyl carbonate (DMC) (1:1 by mass), with 1 M $LiPF_6$ (Merck LP30, Selectipur)]. Cells were assembled in an argon-filled glove box with less than 1 ppm of oxygen and water contents.

Both the cyclic voltammetry (CV) and galvanostatic measurements were performed by means of a computer-controlled cell capture (CCCC) system (Astrol Electronics AG, Oberrohrdorf, Switzerland), by discharging (insertion of lithium-ions) first from respective open-circuit potential. CV measurements were conducted in the range of 1.5–4.0 V vs Li/Li^+ at a potential scan rate of 0.1 mV s^{-1}. Unless otherwise noted, the electrodes were cycled galvanostatically in the range of 2.0–4.0 V vs Li/Li^+ at a specific current of 100 mA g^{-1} (based on the oxide weight). In order to promote complete discharge–charge at the respective potential limits, a potentiostatic step was included until the current was 10% of the current used in the galvanostatic step.

Results and Discussion

Material characterization.— An initial investigation into the synthesis capabilities of FSP was conducted by varying the molar concentration of the precursor solutions. Six different powders were produced from precursors with molar concentrations ranging from 1.50 to 0.25 M, with variations of 0.25 M between each precursor solution. Little change in SSA was seen for powders flame-sprayed from precursor solutions with 1.50 to 0.50 M concentrations, as the BET SSA varied from 33.6 to 39.5 m^2 g^{-1}. A significant increase in the SSA was only seen for powders flame-sprayed from the precursor solution with 0.25 M concentration. Here, a BET SSA of 67.4 m^2 g^{-1} was measured, suggesting that even smaller particles are possible when more dilute precursor solutions are used. From an industrial viewpoint, a higher concentration is more attractive due to the increase in powder production rate.

Material and electrochemical characterizations of the powders produced by FSP of the 1.00 M precursor solution are presented in this work as they are representative of the properties of the FSP-produced LiV_3O_8 nanoparticles. Temperatures before the filter were measured between 150 and 200 °C and amorphous powder with some crystalline features (see Fig. 1a) was collected. By moving the filter paper closer to the flame, the temperatures increased to a range between 250 and 300 °C, and so the powder was annealed above the flame on the filter (see Fig. 1b). The total production time of this batch lasted about 30 min; therefore, the annealing of this material was no longer than 30 min. The crystallinity of this powder can be further refined by subsequent annealing in an oven for 30 min at 350°C (see Fig. 1c). The BET SSA of the amorphous powder was measured to be 35.9 m^2 g^{-1}. This area decreased with increasing heat treatment: 30.5 and 27.5 m^2 g^{-1} for the powder annealed on the filter and subsequently in the oven, respectively.

XRD patterns of the LiV_3O_8 nanoparticles are shown in Fig. 1. For the as-synthesized material (Fig. 1b) a main monoclinic phase is present, while an amount of impurity is also detectable. For the monoclinic phase, the diffraction peak positions for the LiV_3O_8 nanoparticles (lattice constants $a = 6.634$ Å, $b = 3.593$ Å, $c = 11.998$ Å, and $\beta = 107.830°$) match well with those of the known monoclinic layered-type LiV_3O_8 (lattice constants $a = 6.68$ Å, $b = 3.60$ Å, $c = 12.03$ Å, and $\beta = 107.83°$; JCPDS Card No. 72–1193).[19] The corresponding *hkl* indices are given in Fig. 1. Analysis of the XRD data in Fig. 1b and c indicates that the powder is crystalline; however, β-$Li_{0.33}V_2O_5$ is detectable in Fig. 1b as an impurity in the powder, as seen by the peak between 12 and

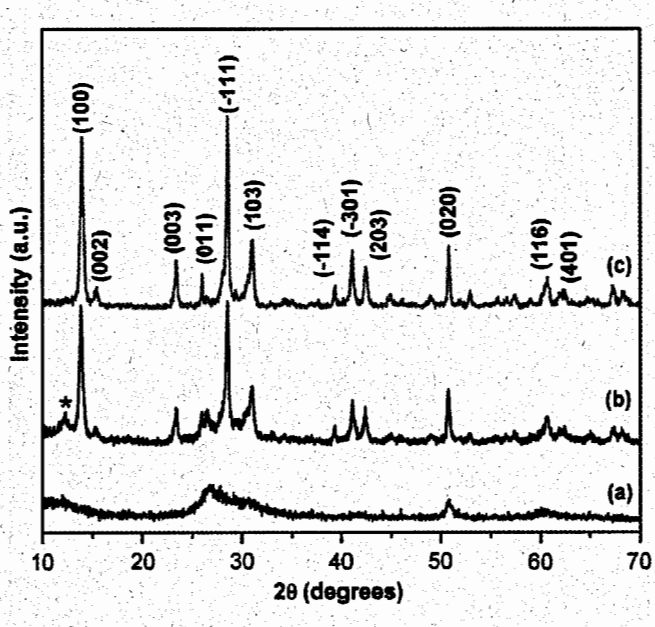

Figure 1. (Color online) XRD of the LiV_3O_8 nanoparticles synthesized by FSP for: (a) amorphous powder, (b) crystalline powder annealed during flame synthesis, and (c) crystalline powder following subsequent annealing at 350°C. The peak beneath the asterisk (*) indicates the presence of β-$Li_{0.33}V_2O_5$.

13° and also in related work.[20] The intensity of this peak significantly decreases upon subsequent heat treatment (Fig. 1c). When the Debye–Scherrer equation was applied to the (100), (020), and (003) peaks in Fig. 1b, the crystallite size of the LiV_3O_8 nanoparticles was calculated as 23.9, 24.0, and 27.5 nm, respectively. The average crystal size is therefore about 25 nm.

The overall morphology of the LiV_3O_8 nanoparticles of the crystalline powder annealed on the filter was investigated by SEM and TEM. The average primary particle diameter observed in the SEM image (Fig. 2a) is approximately 50 nm. Moreover, the particles are agglomerated in chainlike aggregates of primary particles connected by sintered necks and secondary particles clumped together, obviously by van der Waals surface forces. High-resolution transmission electron microscope (HRTEM) images of the LiV_3O_8 nanoparticles synthesized via FSP are shown in Fig. 2b. The strongly crystalline structure of the flame-spray pyrolyzed LiV_3O_8 nanoparticles is well-defined by the highlighted lattice constant c (1.2 nm). Moreover, the corresponding selected area electron diffraction (SAED) pattern for the flame-spray pyrolyzed LiV_3O_8 nanoparticles is shown in the inset of Fig. 2b, revealing the *hkl* indices of the LiV_3O_8 nanoparticles, which is in accordance with the monoclinic phase of LiV_3O_8 (JCPDS Card No. 72–1193). A Li/V ratio in the powder was calculated to be 1.01/3.00 based on ICP-OES measurements. When considering the accuracy of the analytical method, this is in good agreement with the 1/3 stoichiometric ratio of Li/V used in the solution precursor prepared prior to the flame synthesis. Because of the excellent agreement between the XRD data and the known monoclinic layered-type LiV_3O_8, the analysis by HRTEM, and a calculated Li/V ratio of 1.01/3.00, this powder consists primarily of LiV_3O_8 and the material and electrochemical contributions of other phases are assumed to be insignificant. Impurities such as β-$Li_{0.33}V_2O_5$ could, however, have a minor influence on the electroactivity of the powder.

The BET SSA of the as-synthesized crystalline powder was measured to be 30.5 m^2 g^{-1}. This is much higher than those values (<6 m^2 g^{-1}) for sub-μm particles that are produced by spray drying,[21] and shows that FSP is superior when small particles are required at an industrial scale. In order to confirm the degree of porosity in our as-synthesized LiV_3O_8 material, a standard N_2

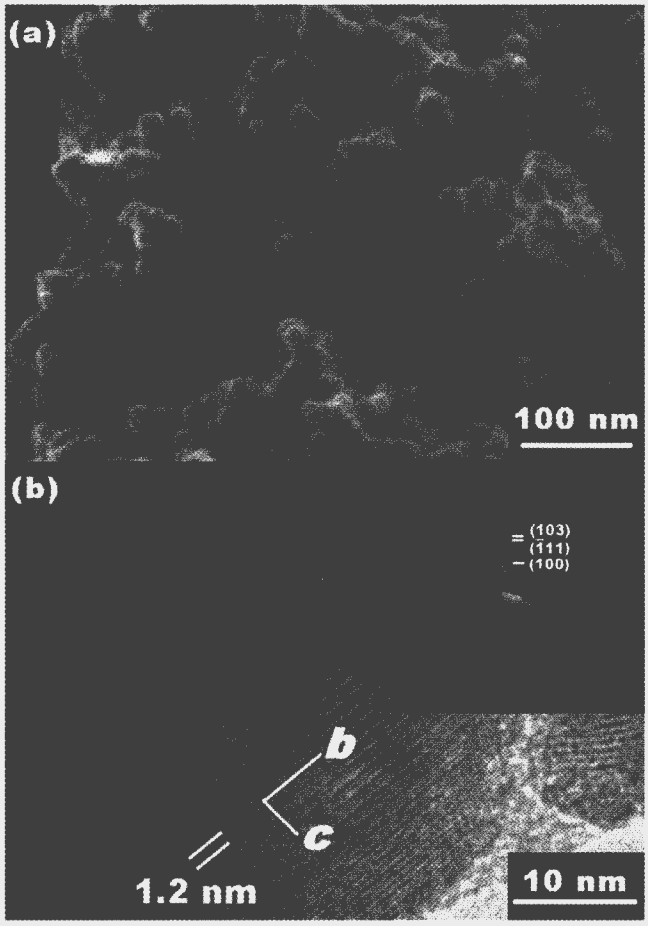

Figure 2. (a) SEM image of the LiV_3O_8 nanoparticles synthesized by FSP. (b) HRTEM image of the LiV_3O_8 nanoparticles synthesized by FSP. Inset displays the corresponding SAED pattern for image (b). The *hkl* indices of the diffuse rings are listed based on JCPDS Card No. 72–1193.

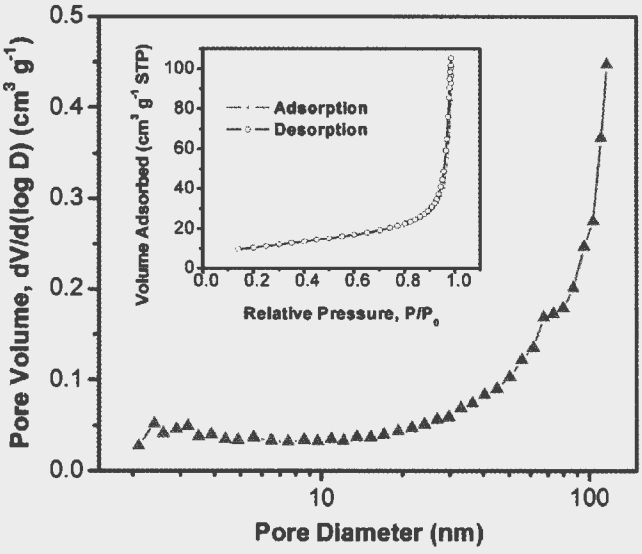

Figure 3. (Color online) Pore size distribution curve of the FSP-made LiV_3O_8 nanoparticles, calculated from the adsorption points using the BJH algorithm. Inset shows the corresponding N_2 adsorption–desorption isotherms.

adsorption–desorption isotherm test was carried out on a Micromeritics Tristar 3000 adsorption apparatus at 77 K. Figure 3 shows the pore size distribution curve calculated from the adsorption points using the Barrett–Joyner–Halenda (BJH) algorithm. Only the presence of macropores is evidenced here, resulting from the particle interfaces. The average pore diameter calculated from the BJH adsorption curve was 15.3 nm, which is about one third of the size of a LiV_3O_8 particle. The low degree of porosity was further verified by the corresponding N_2 adsorption–desorption isotherms (see the inset of Fig. 3), where no hysteresis loop was observed at low relative pressures, indicating the presence of macropores only.

Electrochemical characterization.— The electrochemistry of the LiV_3O_8 crystalline nanoparticles is studied only for the powder annealed during flame synthesis. Cyclic voltammograms of the LiV_3O_8 powder are shown in Fig. 4 for the second and 20th cycle. The oxidative and reductive peaks are seen to diminish rapidly from the second to the 20th cycle due to capacity fading. The shapes of these two voltammograms are roughly the same. Assuming there is no second phase developing and simultaneously not modifying the cyclic voltammogram, than no significant change in the crystallography is expected between these cycles. This would indicate that the decrease in the specific capacity is likely due to the loss of the electrochemically active mass. Possible losses could be due to the dissolution of LiV_3O_8 into the electrolyte,[7] formation of an insulating passivation layer between the active material particles and the electrolyte,[22] and/or the degradation of the electrode composite resulting in a contact loss, possibly due to the growth of the insulating passivation layer. A simple qualitative observation of the dissolution of the powder was done by placing the powder into a 1 M $LiPF_6$, EC:DMC (1:1 by weight) electrolyte. After 1 month of storage in the liquid electrolyte, the initially clear solution was seen to be colored. This confirms that a dissolution of the powder occurs, but not necessarily at a rate that would significantly influence capacity fading. Tanguy et al. associate the capacity fading with the buildup of a passivation layer between the electrode and electrolyte, which was seen to contain organic species as indicated by X-ray photoelectron spectroscopy measurements.[22] This is likely occurring during the cycling of the electrodes presented in this work, as the active material is similar to the material used by Tanguy et al. in terms of average particle size.

Upon repeated cycling, a broad peak at around 3.1 V in the 20th cycle appears. This indicates that an additional oxidative reaction is occurring at a higher potential value than initially experienced. A similar event was experienced by another group,[22] but its occurrence also was not understood.

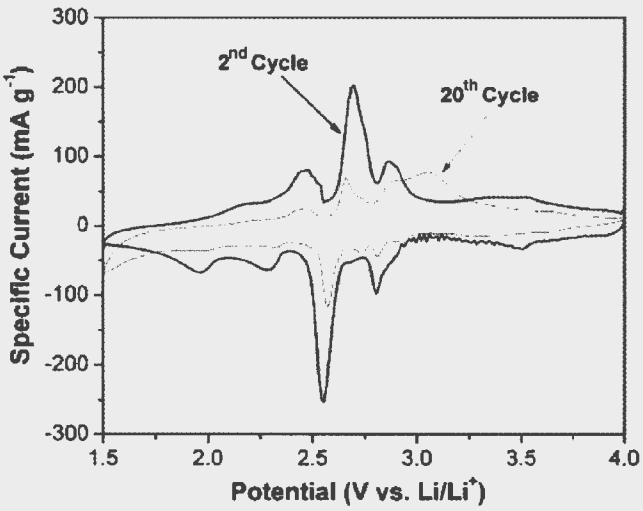

Figure 4. (Color online) Cyclic voltammograms of LiV_3O_8 at the second and 20th cycle at 0.1 mV s^{-1}.

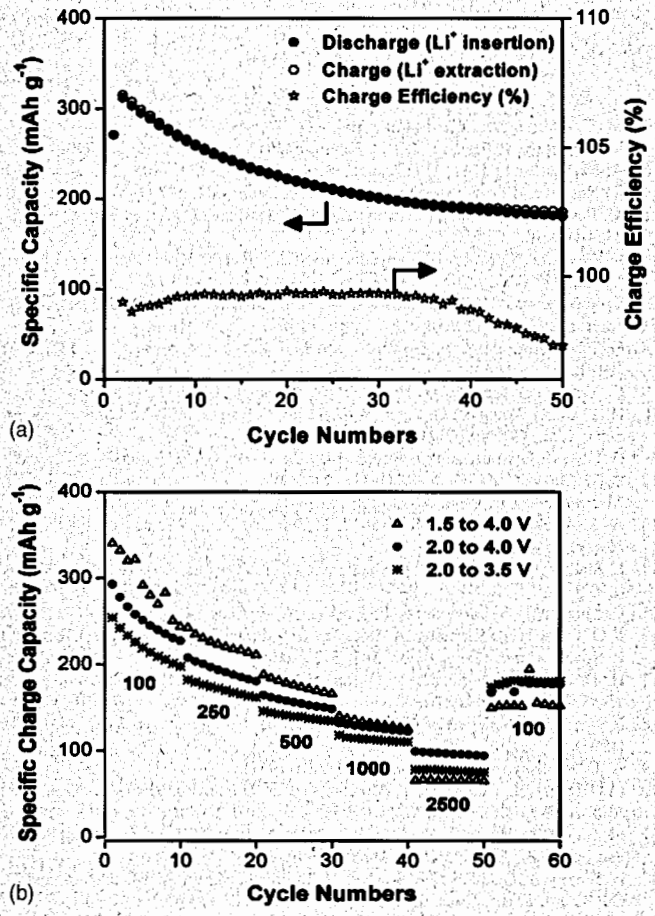

Figure 5. Cycle life behavior for an electrode with the FSP-produced LiV_3O_8 nanoparticles at (a) 100 mA g^{-1}, with cutoff potentials of 2.0 and 4.0 V, and (b) at different specific current densities with various cutoff potentials. The numbers indicate the specific current in mA g^{-1}.

Figure 5a shows the cycling behavior of the LiV_3O_8 electrode. A cycling procedure was used between 2.0 and 4.0 V vs Li/Li^+ at a specific current of 100 mA g^{-1}. The first discharge (Li^+ insertion) was performed from the open-circuit potential of about 3.3 V, corresponding to a specific discharge capacity of 271 mAh g^{-1}. This was then followed by charging (Li^+ extraction) to a potential of 4.0 V, corresponding to a specific charge capacity of 315 mAh g^{-1}. The general trend thereafter is a gradual decrease in the specific capacity. A similar trend is seen in the work of Gao et al.[23] In their work, they described the synthesis and characterization of LiV_3O_8 microparticles (particle size around 2 μm) produced by spray drying. This powder also exhibits a high initial capacity (>300 mAh g^{-1}) and gradual capacity fading. They attribute the high capacity to the structure of the particles, and connect the capacity fading with outstanding structural changes during the lithium insertion and extraction process.

Engineering of the electrode could decrease the capacity fading. It has been seen in other work that the preparation of the electrode can play an important role in the cycling capacity of an active material.[24] The high BET SSA of the material presented in this work (>30 m^2 g^{-1}) likely leads to capacity-decreasing side reactions occurring between the active material and electrolyte as seen in related work.[22]

The dependence of the specific capacity on the current density and potential cutoff is shown in Fig. 5b. For all varied potential cutoff, the discharge capacity decreased as the current density increased. However, for the LiV_3O_8 nanostructured electrode cycled between 2.0 and 4.0 V vs Li/Li^+, it demonstrated good rate capabilities, even up to 2500 mA g^{-1}, retaining a discharge capacity above 100 mAh g^{-1}. This is likely occurring because the increase in lithium extraction has an irreversible reaction mechanism against lithium insertion.[25] This is particularly apparent during high current densities where capacity fading is seen to increase in comparison to the other two measurements. This decline leads to a lower capacity beyond 50 cycles, where the specific current returns to its original value of 100 mA g^{-1}. Capacity fading is clearly strongest for specific currents greater than 1000 mA g^{-1} for potential cutoffs of 1.5 and 4.0 V.

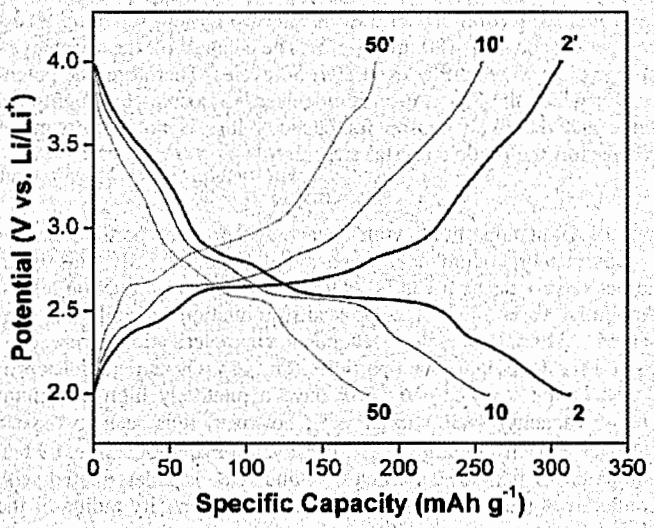

Figure 6. (Color online) Second, tenth, and 50th cycle discharge–charge plots of LiV_3O_8 electrode. Cycling took place between 2.0 and 4.0 V vs Li/Li^+ at 100 mA g^{-1}.

The influence of the particle size is a likely candidate for the pronounced capacity fading seen in our case. The work of Kannan and Manthiram[3] presents LiV_3O_8 particles with sizes of 4 μm produced via a solution dispersion method. This powder was measured to have a specific capacity of 230 mAh g^{-1} with no significant fading after 20 cycles when cycled at 0.5 mA cm^{-2} between 2.0 and 3.5 V. The improved cycling of this material over the one presented in our paper is likely better because the μm-sized particles experience weaker capacity-decreasing side reactions than the nano-sized particles do. To overcome this disadvantage, Chew et al.[12] coated their LiV_3O_8 nanoparticles (50 nm from XRD) produced via a low-temperature solution route with polypyrrole (PPy). The result is almost no capacity fading upon cycling: a reversible capacity of 183 mAh g^{-1} after 100 cycles with PPy-coated material as compared to a decrease from over 200 to 110 mAh g^{-1} for uncoated material. Both materials were cycled at 40 mA g^{-1} between 1.50 and 3.85 V. This result suggests that coating with a conductive binder can significantly inhibit the capacity fading for LiV_3O_8 nanoparticles and would likely decrease the rate of formation of a passivation layer expected at the electrode/electrolyte interface.[12]

In this work, the charge efficiency (%) shown in Fig. 5 is defined as follows

$$\text{Charge efficiency (\%)} = \left(100 - \frac{C_C - C_D}{C_C} \times 100\right) \quad [1]$$

where C_C and C_D are the charge and discharge capacities (specific capacity), respectively.

Figure 6 summarizes the second, tenth, and 50th electrochemical lithiation (discharge)/delithiation (charge) capacity data for the LiV_3O_8 electrode. The calculated specific capacities were solely based on the active material, LiV_3O_8 nanoparticles. The LiV_3O_8 electrode shows a capacity fading behavior upon prolonged cycling. However, the LiV_3O_8 electrode still maintained fairly high Li-ion

insertion/deinsertion capacity even after 50 cycles, retaining a discharge capacity of 180 mAh g^{-1}. The shapes of the discharge–charge plots were similar even after 50 cycles. Therefore, the potentials at which the Li-ion insertion/deinsertion occurs are roughly the same and the likely reason for capacity loss is not due to major changes in the oxide's crystal structure.

Conclusion

LiV_3O_8 nanoparticles with an average primary particle size of approximately 50 nm have been synthesized by FSP. This is an attractive process as it can be scaled to industrial production levels. An initial variation of the lab-scale production capability is presented. Material and electrochemical characterizations were conducted for the LiV_3O_8 nanoparticles. The LiV_3O_8 nanoparticles produced in the dry phase by FSP have a relatively high maximum charge capacity (>300 mAh g^{-1}); however, it is seen to have a stronger capacity fading (>2% per cycle beyond 50 cycles) when compared to μm-sized particles[3,21] and nanoparticles treated with conductive binders.[12] Possible sources of the capacity fading of the electrodes containing the FSP-produced nanoparticles are the formation of a passivation layer at the electrode/electrolyte interface, dissolution of the active material into the electrolyte, and/or insufficient engineering to optimize the electrode composition. Nevertheless, LiV_3O_8 nanoparticles are promising as cathode materials for use in lithium batteries, and further investigations will follow.

Acknowledgments

Scientific discussions with and continuous support from Professor Sotiris E. Pratsinis (ETH Zurich) and Professor Alexander Wokaun (PSI and ETH Zurich) are gratefully acknowledged. Technical assistance from Werner Scheifele (PSI) and Hermann Kaiser (PSI) is appreciated. This research was partially supported by ETH research grant TH-29/05-2. S.H. Ng thanks the ARC Centre of Excellence funding under the grant number CE0561616, for providing financial support during his Ph.D. studies at the University of Wollongong, Australia. We thank the Electron Microscopy Center of the ETH Zurich (EMEZ) for providing the necessary infrastructure.

The Paul Scherrer Institut assisted in meeting the publication costs of this article.

References

1. M. S. Whittingham, *Chem. Rev.*, **104**, 4271 (2004).
2. M. Broussely, P. Biensan, and B. Simon, *Electrochim. Acta*, **45**, 3 (1999).
3. A. M. Kannan and A. Manthiram, *J. Power Sources*, **159**, 1405 (2006).
4. K. Nassau and D. W. Murphy, *J. Non-Cryst. Solids*, **44**, 297 (1981).
5. M. Pasquali, G. Pistoia, V. Manev, and R. V. Moshtev, *J. Electrochem. Soc.*, **133**, 2454 (1986).
6. J. Kawakita, T. Kato, Y. Katayama, T. Miura, and T. Kishi, *J. Power Sources*, **81–82**, 448 (1999).
7. S. Jouanneau, A. L. G. La Salle, A. Verbaere, and D. Guyomard, *J. Electrochem. Soc.*, **152**, A1660 (2005).
8. G. Pistoia, M. Pasquali, G. Wang, and L. Li, *J. Electrochem. Soc.*, **137**, 2365 (1990).
9. G. Yang, G. Wang, and W. Hou, *J. Phys. Chem. B*, **109**, 11186 (2005).
10. H. Y. Xu, H. Wang, Z. Q. Song, Y. W. Wang, H. Yan, and M. Yoshimura, *Electrochim. Acta*, **49**, 349 (2004).
11. D. Guy, B. Lestriez, and D. Guyomard, *Adv. Mater.*, **16**, 553 (2004).
12. S. Y. Chew, C. Q. Feng, S. H. Ng, J. Z. Wang, Z. P. Guo, and H. K. Liu, *J. Electrochem. Soc.*, **154**, A633 (2007).
13. A. S. Arico, P. Bruce, B. Scrosati, J. M. Tarascon, and W. van Schalkwijk, *Nat. Mater.*, **4**, 366 (2005).
14. L. Mädler, H. K. Kammler, R. Mueller, and S. E. Pratsinis, *J. Aerosol Sci.*, **33**, 369 (2002).
15. R. Mueller, L. Mädler, and S. E. Pratsinis, *Chem. Eng. Sci.*, **58**, 1969 (2003).
16. F. O. Ernst, H. K. Kammler, A. Roessler, S. E. Pratsinis, W. J. Stark, J. Ufheil, and P. Novák, *Mater. Chem. Phys.*, **101**, 372 (2007).
17. H. D. Jang, C. M. Seong, Y. J. Suh, H. C. Kim, and C. K. Lee, *Aerosol Sci. Technol.*, **38**, 1027 (2004).
18. P. Novák, W. Scheifele, F. Joho, and O. Haas, *J. Electrochem. Soc.*, **142**, 2544 (1995).
19. A. D. Wadsley, *Acta Crystallogr.*, **10**, 261 (1957).
20. M. Dubarry, J. Gaubicher, P. Moreau, and D. Guyomard, *J. Electrochem. Soc.*, **153**, A295 (2006).
21. N. Tran, K. G. Bramnik, H. Hibst, J. Prölß, N. Mronga, M. Holzapfel, W. Scheifele, and P. Novák, *J. Electrochem. Soc.*, Submitted.
22. F. Tanguy, J. Gaubicher, P. Soudan, N. Bourgeon-Martin, V. Mauchamp, and D. Guyomard, *Electrochem. Solid-State Lett.*, **10**, A184 (2007).
23. H. Gao, C. Y. Jiang, and C. R. Wan, *J. Power Sources*, **125**, 90 (2004).
24. D. Guy, B. Lestriez, R. Bouchet, V. Gaudefroy, and D. Guyomard, *Electrochem. Solid-State Lett.*, **8**, A17 (2005).
25. J. Kawakita, T. Miura, and T. Kishi, *Solid State Ionics*, **118**, 141 (1999).